

# Cryogenic Temperature Properties and Secondary Phase Characterization of CuCrZr Composites

Rongmei Niu, Vince Toplosky, and Ke Han

**Abstract**—We achieved both high electrical conductivity and high mechanical strength in CuCrZr wires, which are comparable to those of Al60 at both 295 K and 77 K. The ultimate tensile strength (UTS) was above 602 MPa at 295 K. The room temperature conductivity was 84 % IACS with a residual-resistivity ratio (RRR at 77 K) of 3.57. The wires fabrication included solid solution treatment, aging treatment, and cold drawing. The sequence of the aging and cold drawing after solid solution had not obvious influence on the final UTS and conductivity. At micron scale, the composite wires were composed of a high volume-fraction of Cr-rich secondary phases embedded in Cu matrix. Those Cr-rich particles demonstrated appreciable co-deformation capability with the Cu matrix during cold drawing, which was beneficial significantly to wire fabrication in decreasing the chance of de-cohesion and avoiding cracks during cold deformation. Large amount of Cr precipitates formed after aging, which significantly decreased the Cr content dissolved in Cu matrix, thereby, contributed to the high conductivity in CuCrZr composites.

**Index Terms**—High electrical conductivity, CuCrZr, cold deformation, co-deformation, pulsed magnet.

## I. INTRODUCTION

Cu-based composites are widely used in magnets as conductor materials because of their achievable electrical conductivity and high mechanical strength. Typical conductors are Cu-based metal-metal composites, such as Cu–Ag[1-3], Cu–Nb[4-7], and metal matrix composite reinforced by particles (Cu–alumina)[1, 8, 9].

High strength is usually incompatible with high conductivity. The ultimate strength values of CuAg and CuNb composites[10] used in magnets are around 900 MPa and over 1.1 GPa respectively. The room temperature conductivity is ~74 %IACS, and ~65 %IACS (international annealed copper standard) in each case. By contrast, Cu-1.1 wt% alumina, (Glidcop Al60) composites have modest strength increase relative to pure Cu (~550 MPa) but maintain a better conductivity ~83 % IACS[9]. Therefore, Al60 are most suitable for high field magnet coils that require high conductivity.

The fabrication of Al60 conductors requires high deformation strain. It is, however, challenging to draw without breakage, which is often associated with chevron cracks created prior to the breakage. In our previous work[9, 11], we reported the inhomogeneous distribution of alumina particles and the presence of large particles. Large particles are unable to co-

deform with matrix and reduce the deformability of wire. Because of inhomogeneity of particle distribution in Al60, many mechanical tests must be conducted before these conductors can be used in magnets.

To develop an alternative for Al60, we studied CuCrZr composites. CuCrZr composites were developed by alloying with traces of Cr and Zr elements. The maximum solubility of Cr in Cu is approximately 0.7 wt% (0.89 at%) at 1077 °C and falls to near zero at room temperature[12, 13]. The good conductivity was attribute to the very low solubility of Cr and Zr in Cu at room temperature. In Cu–0.5Cr wt% alloy, researchers obtained a combination of 84 %IACS conductivity and 550 MPa strength via four passes of equal channel angular processing (ECAP) followed by cold rolling and aging[14]. In Cu–0.44Cr–0.2Zr wt% alloy, other researchers achieved tensile strength 650 MPa and electrical conductivity 81 %IACS after eight ECAP passes and aging treatment[15]. In vast numbers of papers and data, CuCrZr alloys generally demonstrated a strength ~ 550 MPa[16], and electrical conductivities in the 75 to 80 %IACS range[12, 14, 15, 17-19]. Obviously, this combination of strength and conductivity needs to improve further to meet the requirements of middle pulsed magnets.

In this work, CuCrZr conductor wires were made by cold drawing, and two routes were followed: Solution treating + Aging + Cold-drawing, and Solution treating + Cold-drawing + Aging.

For conductors used in pulsed magnets, both mechanical properties and electric conductivity at cryogenic temperature, which have not been reported before on this kind of composites, are very critical. Accordingly, in present work, we explored the mechanical properties and conductivity of CuCrZr composites at 77K.

The secondary phase particles in the CuCrZr composite may reduce the deformability. We therefore investigated the morphology and composition of these particles.

## II. EXPERIMENTAL METHODS

### A. Materials and Fabrication

The investigated alloy had a composition of Cu-0.54Cr–0.046Zr alloy (wt%). This material, received in an age-hardened state, was used as one initial condition for the hardening and electrical conductivity studies. Cold drawing was conducted to achieve a designed dimension (a cross section

The work was supported in part by the National Science Foundation under Grant DMR-1157490, in part by the State of Florida, and in part by the U.S. Department of Energy. (Corresponding author: Ke Han.)

R.Niu, V. Toplosky, and K. Han are with the National HighMagnetic Field Laboratory, Tallahassee, FL 32309 USA (e-mail: [han@magnet.fsu.edu](mailto:han@magnet.fsu.edu)).

Color versions of one or more of the figures in this article are available online at <http://ieeexplore.ieee.org>

> Manuscript ID MT27-681<

area of 6.7 mm x 11.0 mm, total drawing true strain,  $\eta=1.10$ ) used in pulsed magnets. The deformation true strain,  $\eta$ , was defined as  $\ln(A_0/A_1)$ , where  $A_0$  is the original area and  $A_1$  is the final area after reduction.

Meanwhile, to understand the evolution of properties including mechanical strength and electrical conductivity, we solution treated another batch of as-received bar with the same nominal composition at 1000 °C for 2 hours followed by a water quench. The solution-treated bars with a diameter of 8mm was heavily drawn to a x-section of 0.8 mm x 1.2 mm ( $\eta=3.97$ ). Subsequently, the drawn wire was aged at 425°C up to 4 h in an argon atmosphere with 1% hydrogen. In paragraphs below, we named the large x-section CuCrZr, 6.7 mm x 11.0 mm, CCZL and the small x-section, 0.8 mm x 1.2 mm, CCZS.

### B. Microstructure Examination

Microstructure was investigated in a FEI Helios G4 UC multi-technique dual beam (electron and Ga ion) Field Emission Scanning Electron Microscope (FESEM) at an accelerating voltage of 10 kV or 15 kV. For chemistry examinations, an Energy Dispersion X-ray (EDX) spectrometer was attached.

Samples for transmission electron microscopy (TEM) were prepared by twin-jet polishing (TUNEPOL 3-Struers) using in a mixture of 30 % phosphoric acid and 70 % deionized water at 295K. High-angle-annular-darkfield STEM (HAADF STEM) studies were carried out on a probe-aberration-corrected, cold-field-emission JEM JEOL ARM 200cF at 200 kV. HAADF-STEM images were acquired using a 30- $\mu$ m condenser lens aperture, at a camera length of 8 cm corresponding to a collection angle of 58.7 mrad. The mage-scanning speed was 32  $\mu$ s/pixel. The beam convergent angle was 21 mrad. EDS was done using the Oxford Aztec system in STEM.

### C. Mechanical Tests

Tensile tests were performed at 295 K and 77 K in displacement control at a rate of 0.5 mm/min on a servo-hydraulic MTS machine. An unload/reload cycle was used at 1.5 % strain to determine elastic modulus. A 25-mm clip-on extensometer was used to record strain. The final elongation was determined by measuring the edge grip-to-grip distance before (nominally 50 mm) and after sample failure.

### D. Electrical Conductivity Measurements

The conductivity measurements were performed by a standard four-point method on samples with a nominal length of 150 mm. Voltage taps were mechanically clamped on the specimens at a distance of approximately 100 mm. Current leads were attached to the ends of the specimens with input current values of 0.25, 0.50, 0.75 and 1.0 amps. The procedure was then repeated at 77 K in a liquid-filled dewar. The values reported here were estimated with an error within +/- 1% IACS.

## III. RESULTS AND DISCUSSIONS

### A. Mechanical Properties and Conductivity

Mechanical tests showed that samples were about 20% stronger at 77k than at 295 K (Table 1). In CCZL wire, the ultimate strength (UTS) at room temperature was 614 MPa which increased to 744 MPa at 77 K (a 21% increase). In CCZS, the UTS was almost identical with the CCZL. The yield strength in CCZS, however, was reduced by 6 % and 10 % at 295 K and 77 K, respectively, though CCZS wire was subject to more drawing strain than the coarse one. The reason for the reduced yield strength and identical UTS at higher drawing true strain may be attribute to dynamic recovery occurred in CCZS during heavily drawing deformation[16, 18, 20, 21]. The UTS/YS ratio in the CCZL was less than that in CCZS at both 295 K and 77 K, indicating higher strain hardening rates in CCZS, especially at 77 K. Furthermore, the elongation was longer in CCZS. Both the high strain hardening rate and large elongation in CCZS wire confirmed the reduced dislocation density caused by dynamic recovery during cold drawing.

Comparing with Al60, CuCrZr wires in our current work demonstrated higher yield strength, tensile strength, Young's modulus at both 295 K and 77 K. The strain hardening rate in CCZS and Al60 were closer to each other.

TABLE I  
TENSILE TEST RESULTS IN CUCRZR WIRES WITH DIFFERENT X-SECTION AREA

mm x mm	T (K)	E (GPa)	YS (MPa)	UTS (MPa)	UTS /YS	Ef (%)
CuCrZr						
6.7x11	295	123±0	612±2	614±0	1.00	9.0±0.3
6.7x11	77	131±2	711±4	744±7.8	1.05	19.8±0.6
0.8x1.2	295	129±2	577±16	614±17	1.06	10.6±1.4
0.8x1.2	77	140±2	642±16	750±12	1.17	23.7±0.5
Al60						
6.7x11	295	114±2	532±7	564±5	1.06	12.1±1.5
6.7x11	77	127±5	657±4	728±6	1.11	15.7±0.3

T: temperature; E: elastic Young's modulus; YS: yield strength; UTS: ultimate tensile strength; Ef: elongation at fracture.

TABLE II  
ELECTRICAL CONDUCTIVITY IN CUCRZR WIRES

Cross-section, mm x mm	%IACS		RRR
	295 K	77 K	
CuCrZr			
6.7x11	84.2±0.9	322.8±4.8	3.84±0.09
0.8x1.2	85.6±0.2	306.0±0.7	3.57±0.01
Al60			
6.7x11	83.4±0.3	359.8±5.2	4.31±0.06

At 295 K, CCZS wires had slightly higher conductivity than CCZL, but at 77 K, CCZS wires had 5 % lower conductivity, leading to a difference of RRR of 7 % (see Table 2). This difference may be attributed to the combination of dissolution of solute atoms and decreased dislocation density in CCZS.

Comparing with AL60, the conductivity of CuCrZr at 295 K was almost same as that of Al 60. The conductivity of CuCrZr at 77 K was about 10-15 % lower. As resulted in a relatively

> Manuscript ID MT27-681<

low RRR in the CuCrZr. In practical application, the current RRR value in the CuCrZr may cause temperature raise in the magnet coils. We speculate that Al 60 has fewer alloying elements dissolved in Cu matrix. Thus, the conductivity of CuCrZr can be improved by reducing the dissolved alloying elements in the conductor using longer aging time.

In comparison with previous studies[19, 22, 23], our improved room temperature conductivity ( $\sim 85$  %IACS), was not compromised by high UTS (614 MPa at 295 K). Kulczyk et al., achieved higher UTS of 630 MPa at 295K by the optimization of process parameters for hydrostatic extrusion and post-deformation aging[22]. However, the corresponding conductivity was only 78 %IACS, which was lower than the tested value in our current work.

### B. Particle Characterization

In both the CCZL and CCZS, we observed high density of large particles uniformly distributed in the materials. The average particle size and particle spacing by light microscopy were estimated respectively to be  $1.5 \pm 0.9 \mu\text{m}$  and  $8.2 \pm 2.6 \mu\text{m}$  in CCZL on the transversal x-section (Fig.1). In the drawn CCLS, we observed the existing of these particles even before the aging. From our another work [24], we discovered that those particles started to present after the solid-solution treatment.

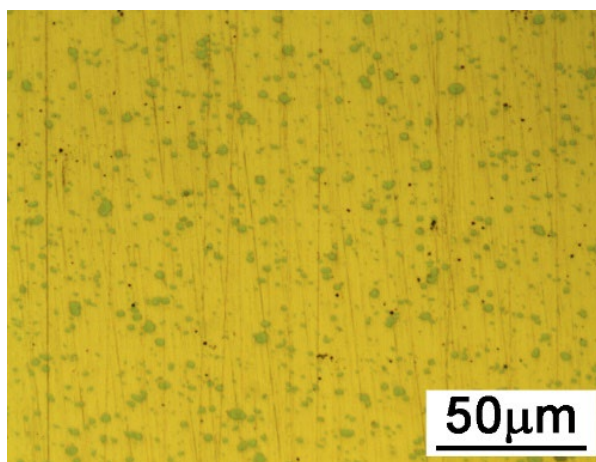


Fig. 1. Light microscopy observation on large particles along transversal section in CCZL(6.7 mm x 11 mm) wire.

We compared the particles morphology along the wire drawing direction. The length over width ratios were in a range of 1-2 when the wire was in a diameter of 14 mm. While the ratio increased to 1-100 when the wire was subjected to 55% reduction-in-area (RA) to 6.7 mm x 11.0 mm (Cf. Fig.2(b), Fig. 3(a) and 3(b)). Obviously, particles were elongated with drawing.

Using SEM-EDS, we found that the elongated ribbons or fibers on the drawing direction were composed of mainly Cr, see Fig. 3 and Table 3. The atomic ratio of Cr/Cu fiber particle was up to 90:9. Wide fibers or big particles had higher Cr content than fine fibers or small particles ( $< 2 \mu\text{m}$  in width or

diameter). At fine fibers or small particles, the “decreased” Cr content may be restricted by the SEM-EDS spatial resolution, because more signal came from the Cu matrix when secondary phase particle became small.

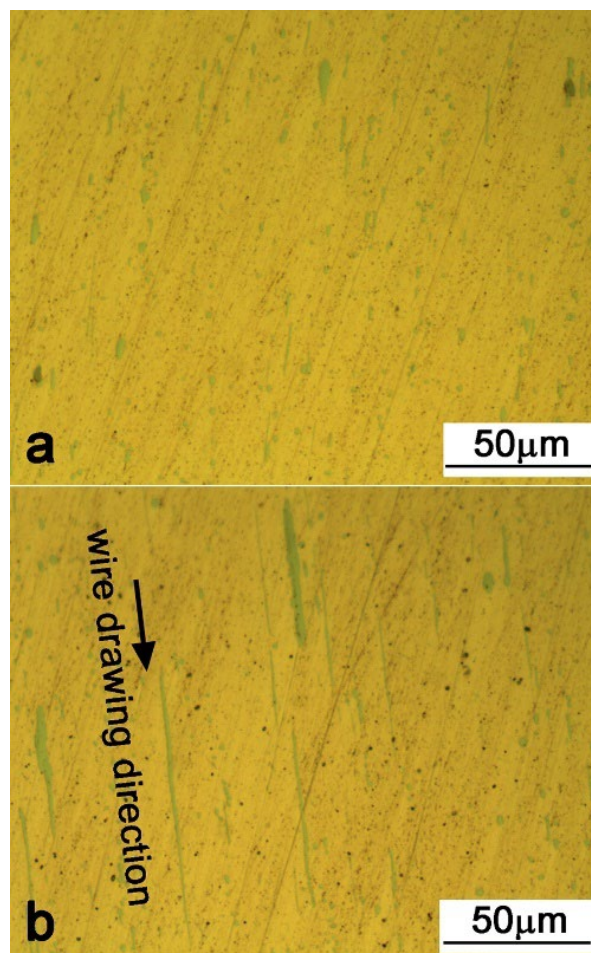


Fig. 2. Light microscopy observation on large particles along longitudinal section. (a) in dia.14 mm wire. (b) in 6.7 mm x 11.0 mm wire. Particles were obviously elongated along wire drawing direction.

The SEM-EDS elemental mapping along drawing direction exhibited a continuous Cr distribution in the long fibers in Fig. 4. Combining with the observation in Figs. 2 and 3, we believed that Cr-rich particles were well co-deformed with the Cu matrix during cold deformation. In Verhoeven’s work, it was reported that the Cr ribbon was able to be cold-drawn to a strain of 8.3[25] without breakage. Therefore, the existing of large or small Cr-rich particles would not be the source of cracks or decohesion, and not result in drawing issues in wire production.

Cr-rich secondary phases had various shapes, from long fibers to round particles, and had a very wide size distribution from hundreds of nanometers to tens of micrometers. Cr particles exhibited well co-deformation properties with matrix.

Zr-rich particles were very scattered because of the low content (0.046 wt%). The morphology of those particles was irregular, and their size was usually several micrometers. They appeared brittle and demonstrated poor co-deformation capability with Cu matrix during cold drawing (Fig. 4). Gaps and fractures were often observed around Zr-rich particles.

> Manuscript ID MT27-681<

In Zr-rich particles, the Zr atomic content was up to 66 %. High Zr contents were always associated with high level of Cr contents. For instance, the atomic ratio of Zr/Cr was 66:18 in Table 3. Cr has a max. solubility of ~ 0.49 at.% in Zr at 836 °C[26]. According to the Zr-Cr system phase diagram, the most probable intermetallic compounds would be Cr<sub>2</sub>Zr[26]. Since the melting points of Zr and Cr are 1855 °C and 1863 °C, respectively, we assume the Cr<sub>2</sub>Zr come from the solidification of the alloy and did not dissolve completely during the homogenization treatment at 1000 °C.

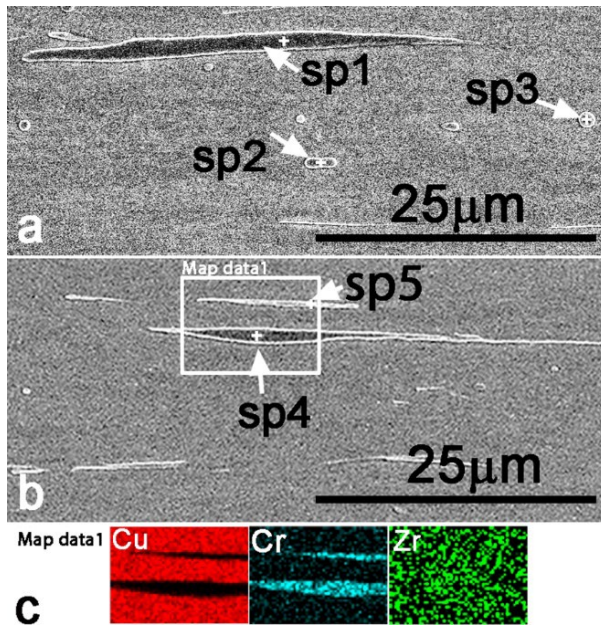


Fig. 3. (a) and (b) SEM observation on the co-deformation capability of Cr-rich and Zr-rich particles along longitudinal section in the 6.7x 11mm<sup>2</sup> wire. Cr-rich particles are elongated along wire drawing direction, and no de-cohesion was observed around Cr-rich particles. The particle positions, sp1 through sp5, for EDS results in Table 3 was indicated by white arrows. (c) EDS mapping.

TABLE III

PARTICLES COMPOSITION ALONG DRAWING DIRECTION.

Element At. %	SP1	SP2	SP3	sp4	sp5	sp6
Cu	9.3	8.0	20.8	0.6	79.1	16.2
Cr	91.6	92.0	78.8	99.4	20.9	18.1
Zr	0.1	0.0	0.4	0.0	0.0	65.7

### C. Precipitates Induced by Aging

Aging treatment produced a high density of precipitates uniformly distributed in the Cu matrix (Fig.5). Because of its low atom number (Z=24), Cr precipitates displayed as a dark contrast in Cu (Z=29) matrix in HAADF images. Their size roughly varied from 1 to 4 nm, which were extremely fine comparing with the matrix grain size of 300 nm. The EDS spectrum on the dark contrast features further verified the presence of Cr. The Cr content was between 1.2 and 8.4 at.%,

which was higher than in the matrix.

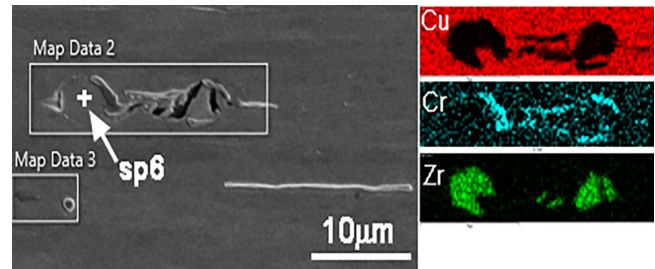


Fig. 4. SEM-EDS mapping on fractured Zr particles (mag data2) along longitudinal section. The position of sp6 in Table 3 was indicated.

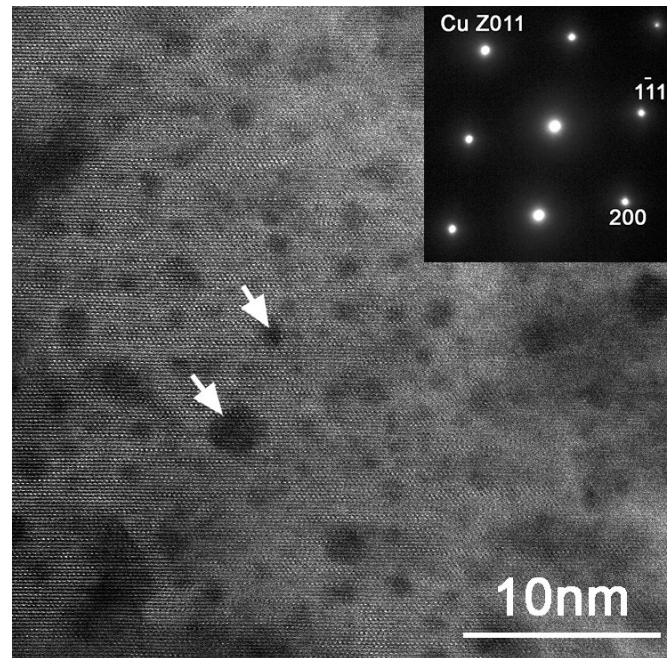


Fig. 5. STEM-HAADF images showing the uniformly distributed Cr precipitates in aged samples. EDS analysis showing the 6.7 at. % and 1.8 at. % Cr content in dark-contrast area, indicated by white arrows. Coherent structure between precipitates with matrix, explained the reason for one set of reflection patten in the selected area diffraction patten in the inset.

## IV. CONCLUSION

Because pulsed magnets operate at 77 K and conductor temperature can reach a value close to room temperature in the same magnet, this current work included mechanical properties at both room and cryogenic temperatures. CuCrZr showed high values for Young's modulus, yield strength, tensile strength, and ductility at 77 K. As is comparable to Al60. It is expected that CuCrZr conductors would perform well when commissioned in high field pulsed magnets operating at 77 K.

### ACKNOWLEDGMENT

We would like to acknowledge B.Starch for drawing, and J. W. Levitan, T. Adkins and E. L. Marks for aging.

> Manuscript ID MT27-681<

#### REFERENCES

- [1] K. Han *et al.*, "Properties of Selected High-Strength Composite Conductors With Different Strengthening Components," *IEEE Transactions on Applied Superconductivity*, vol. 30, no. 4, pp. 1-5, 2020, doi: 10.1109/TASC.2020.2981270.
- [2] C. Zhao *et al.*, "Improvement of properties in Cu–Ag composites by doping induced microstructural refinement," *Materials Science and Engineering: A*, vol. 799, p. 140091, 2021/01/02/ 2021, doi: <https://doi.org/10.1016/j.msea.2020.140091>.
- [3] X. Zuo, K. Han, C. Zhao, R. Niu, and E. Wang, "Precipitation and dissolution of Ag in ageing hypoeutectic alloys," *Journal of Alloys and Compounds*, vol. 622, pp. 69-72, 2015/02/15/ 2015, doi: <https://doi.org/10.1016/j.jallcom.2014.10.037>.
- [4] J. B. Dubois, L. Thilly, F. Lecouturier, P. Olier, and P. O. Renault, "Cu/Nb Nanocomposite Wires Processed by Severe Plastic Deformation for Applications in High Pulsed Magnets: Effects of the Multi-Scale Microstructure on the Mechanical Properties," *IEEE Transactions on Applied Superconductivity*, vol. 22, no. 3, pp. 6900104-6900104, 2012, doi: 10.1109/TASC.2011.2174574.
- [5] L. Thilly, J. Colin, F. Lecouturier, J. P. Peyrade, J. Grilhé, and S. Askénazy, "Interface instability in the drawing process of copper/tantalum conductors," *Acta Materialia*, vol. 47, no. 3, pp. 853-857, 1999/02/05/ 1999, doi: [https://doi.org/10.1016/S1359-6454\(98\)00418-2](https://doi.org/10.1016/S1359-6454(98)00418-2).
- [6] J. D. Verhoeven, H. L. Downing, L. S. Chumbley, and E. D. Gibson, "The resistivity and microstructure of heavily drawn Cu - Nb alloys," *Journal of Applied Physics*, vol. 65, no. 3, pp. 1293-1301, 1989, doi: 10.1063/1.343024.
- [7] K. Han, V. J. Toplosky, R. Walsh, C. Swenson, B. Lesch, and V. I. Pantsyrnyi, "Properties of high strength Cu-Nb conductor for pulsed magnet applications," *IEEE Transactions on Applied Superconductivity*, vol. 12, no. 1, pp. 1176-1180, 2002, doi: 10.1109/TASC.2002.1018611.
- [8] T. J. Miller, S. J. Zinkle, and B. A. Chin, "Strength and fatigue of dispersion-strengthened copper," *Journal of Nuclear Materials*, vol. 179-181, pp. 263-266, 1991/03/01/ 1991, doi: [https://doi.org/10.1016/0022-3115\(91\)90076-J](https://doi.org/10.1016/0022-3115(91)90076-J).
- [9] K. Han, R. E. Goddard, V. Toplosky, R. Niu, J. Lu, and R. Walsh, "Alumina Particle Reinforced Cu Matrix Conductors," *Ieee Transactions on Applied Superconductivity*, vol. 28, no. 3, pp. 1-5, 2018, doi: 10.1109/TASC.2018.2795587.
- [10] K. Han *et al.*, "The fabrication, properties and microstructure of Cu–Ag and Cu–Nb composite conductors," *Materials Science and Engineering: A*, vol. 267, no. 1, pp. 99-114, 1999/07/15/ 1999, doi: [https://doi.org/10.1016/S0921-5093\(99\)00025-8](https://doi.org/10.1016/S0921-5093(99)00025-8).
- [11] J. Lu, T. Adkins, I. Dixon, D. Nguyen, and K. Han, "Nondestructive Testing of High Strength Conductors for High Field Pulsed Magnets," *IEEE Transactions on Applied Superconductivity*, vol. 30, no. 4, pp. 1-5, 2020, doi: 10.1109/TASC.2020.2980525.
- [12] M. Jovanovj and V. Rajkovic, "High electrical conductivity Cu-based alloys, Part I," *Metallurgija*, vol. 15, pp. 125-133, 2009.
- [13] D. J. Chakrabarti and D. E. Laughlin, "The Cr-Cu (Chromium-Copper) system," *Bulletin of Alloy Phase Diagrams*, vol. 5, no. 1, pp. 59-68, 1984/02/01 1984, doi: 10.1007/BF02868727.
- [14] K. X. Wei, W. Wei, F. Wang, Q. B. Du, I. V. Alexandrov, and J. Hu, "Microstructure, mechanical properties and electrical conductivity of industrial Cu–0.5%Cr alloy processed by severe plastic deformation," *Materials Science and Engineering: A*, vol. 528, no. 3, pp. 1478-1484, 2011/01/25/ 2011, doi: <https://doi.org/10.1016/j.msea.2010.10.059>.
- [15] A. Vinogradov, V. Patlan, Y. Suzuki, K. Kitagawa, and V. I. Kopylov, "Structure and properties of ultra-fine grain Cu–Cr–Zr alloy produced by equal-channel angular pressing," *Acta Materialia*, vol. 50, no. 7, pp. 1639-1651, 2002/04/19/ 2002, doi: [https://doi.org/10.1016/S1359-6454\(01\)00437-2](https://doi.org/10.1016/S1359-6454(01)00437-2).
- [16] A. P. Zhilyaev, I. Shakhova, A. Morozova, A. Belyakov, and R. Kaibyshev, "Grain refinement kinetics and strengthening mechanisms in Cu–0.3Cr–0.5Zr alloy subjected to intense plastic deformation," *Materials Science and Engineering: A*, vol. 654, pp. 131-142, 2016/01/27/ 2016, doi: <https://doi.org/10.1016/j.msea.2015.12.038>.
- [17] T. Ellis, S. T. Kim, and J. Verhoeven, "Deformation-processed copper-chromium alloys: Role of age hardening," *Journal of Materials Engineering and Performance*, vol. 4, pp. 581-586, 1995.
- [18] A. Chbihi, X. Sauvage, and D. Blavette, "Influence of plastic deformation on the precipitation of Cr in copper," *Journal of Materials Science*, vol. 49, no. 18, pp. 6240-6247, 2014/09/01 2014, doi: 10.1007/s10853-014-8348-3.
- [19] R. Mishnev, I. Shakhova, A. Belyakov, and R. Kaibyshev, "Deformation microstructures, strengthening mechanisms, and electrical conductivity in a Cu–Cr–Zr alloy," *Materials Science and Engineering: A*, vol. 629, pp. 29-40, 2015/04/01/ 2015, doi: <https://doi.org/10.1016/j.msea.2015.01.065>.
- [20] R. Niu and K. Han, "Strain hardening and softening in nanotwinned Cu," *Scripta Materialia*, vol. 68, no. 12, pp. 960-963, 2013/06/01/ 2013, doi: <https://doi.org/10.1016/j.scriptamat.2013.02.051>.
- [21] R. Niu, K. Han, Z. Xiang, L. Qiao, and T. M. Siegrist, "Ultra-high local plasticity in high-strength nanocomposites," *Journal of Materials Science*, vol. 55, no. 31, pp. 15183-15198, 2020/11/01 2020, doi: 10.1007/s10853-020-05097-1.
- [22] M. Kulczyk *et al.*, "Improved compromise between the electrical conductivity and hardness of the thermo-

> Manuscript ID MT27-681<

- mechanically treated CuCrZr alloy," *Materials Science and Engineering: A*, vol. 724, pp. 45-52, 2018/05/02/ 2018, doi: <https://doi.org/10.1016/j.msea.2018.03.004>.
- [23] L. X. Sun, N. R. Tao, and K. Lu, "A high strength and high electrical conductivity bulk CuCrZr alloy with nanotwins," *Scripta Materialia*, vol. 99, pp. 73-76, 2015/04/01/ 2015, doi: <https://doi.org/10.1016/j.scriptamat.2014.11.032>.
- [24] R. Niu, V. Toplosky, and K. Han, "Deformation-induced precipitation in CuCrZr composites " to be submitted.
- [25] J. D. Verhoeven *et al.*, "Development of deformation processed copper-refractory metal composite alloys," *Journal of Materials Engineering*, vol. 12, no. 2, pp. 127-139, 1990/06/01 1990, doi: 10.1007/BF02834066.
- [26] D. Arias and J. P. Abriata, "The Cr-Zr (Chromium-Zirconium) system," *Bulletin of Alloy Phase Diagrams*, vol. 7, no. 3, pp. 237-244, 1986/06/01 1986, doi: 10.1007/BF02868997.